Chemical Science

ROYAL SOCIETY OF CHEMISTRY

EDGE ARTICLE

View Article Online
View Journal | View Issue

Cite this: *Chem. Sci.*, 2022, **13**, 6233

All publication charges for this article have been paid for by the Royal Society of Chemistry

Harnessing natural-product-inspired combinatorial chemistry and computation-guided synthesis to develop *N*-glycan modulators as anticancer agents†

Wei-An Chen,[a] Yu-Hsin Chen,[a] Chiao-Yun Hsieh,[a] Pi-Fang Hung,[a] Chiao-Wen Chen,[a] Chien-Hung Chen,[a] Jung-Lee Lin,[a] Ting-Jen R. Cheng,[a] Tsui-Ling Hsu,[a] Ying-Ta Wu,[a] Chia-Ning Shen*[a] and Wei-Chieh Cheng *[abcd]

Received 26th October 2021
Accepted 18th April 2022

DOI: 10.1039/d1sc05894k

rsc.li/chemical-science

Modulation of *N*-glycosylation using human Golgi α-mannosidase II (α-hGMII) inhibitors is a potential anticancer approach, but the clinical utility of current α-hGMII inhibitors is limited by their co-inhibition of human lysosomal α-mannosidase (α-hLM), resulting in abnormal storage of oligomannoses. We describe the synthesis and screening of a small library of novel bicyclic iminosugar-based scaffolds, prepared *via* natural product-inspired combinatorial chemistry (NPICC), which resulted in the identification of a primary α-hGMII inhibitor with 13.5-fold selectivity over α-hLM. Derivatization of this primary inhibitor using computation-guided synthesis (CGS) yielded an advanced α-hGMII inhibitor with nanomolar potency and 106-fold selectivity over α-hLM. *In vitro* studies demonstrated its *N*-glycan modulation and inhibitory effect on hepatocellular carcinoma (HCC) cells. *In vivo* studies confirmed its encouraging anti-HCC activity, without evidence of oligomannose accumulation.

Introduction

Protein glycosylation is implicated in numerous biological functions such as cellular development, movement, and recognition;[1,2] and the aberrant distribution patterns of *N*-glycans found in tumor cells are associated with cancer growth and metastasis.[3,4] Human Golgi α-mannosidase II (α-hGMII, EC 3.2.1.114) plays a key role in the modulation of *N*-glycan processing (as part of the *N*-glycan biosynthetic pathway), and its inhibition is known to induce tumor repression.[5–7] For example, *Drosophila* α-GMII (α-dGMII) catalyzes the sequential hydrolysis of two mannoses from $GlcNAcMan_5GlcNAc_2$ to produce $GlcNAcMan_3GlcNAc_2$ – the main precursor of complex type *N*-glycans including the branched *N*-glycans associated with cancer and abnormal cell behavior.[8–11]

The indolizidine alkaloid swainsonine (sw) is a potent but poorly selective α-GMII inhibitor, also inhibiting human lysosomal α-mannosidase (α-hLM, EC 3.2.1.24), causing the accumulation of undegraded oligomannoses in cells or tissues (swainsonine-induced mannosidosis) and limiting its further development (Fig. 1a).[7,12] Although sw derivatives such as 5-substituted sw analogues and other monocylic iminosugars incorporating a pyrrolidine or pyrrolidone skeleton have been investigated, their inhibitory potency and selectivity were all found to be unsatisfactory;[13–17] and crystal structure studies using α-dGMII and bovine lysosomal α-mannosidase (α-bLM) concluded that the key residues in the active site pocket and the zinc coordination involved in sw binding are highly conserved in both enzymes, confounding a simple solution to this vexing selectivity problem.[8,14,18]

One of our research interests is the expeditious development of inhibitors and activators of disease-associated glycoprocessing enzymes.[15,19–21] In previous work, we identified pyrrolidine AN9 incorporating the 2*R*,3*R*,4*S*,5*R* configuration pattern as a potential α-hGMII-inhibiting scaffold, whose C-2 aminomethyl moiety could be well-suited to diversity exploration (Fig. 1b). Herein, we describe the design and synthesis of a series of new bicyclic iminosugar-based scaffolds bearing a diversity position on the polyhydroxylated pyrrolidine substructure, followed by the development of novel α-hGMII inhibitors guided by natural product-inspired combinatorial chemistry (NPICC) and computation-guided synthesis (CGS).

[a]*Genomics Research Center, Academia Sinica, 128, Section 2, Academia Road, Taipei, 11529, Taiwan. E-mail: wcheng@gate.sinica.edu.tw*

[b]*Department of Chemistry, National Cheng-Kung University, 1, University Road, Tainan 701, Taiwan*

[c]*Department of Applied Chemistry, National Chiayi University, 300, Xuefu Rd, East Dist., Chiayi 600, Taiwan*

[d]*Department of Medicinal and Applied Chemistry, Kaohsiung Medical University, 100 Shih-Chuan 1st Rd, Kaohsiung 807, Taiwan*

† Electronic supplementary information (ESI) available. CCDC [2116295-2116296]. For ESI and crystallographic data in CIF or other electronic format see https://doi.org/10.1039/d1sc05894k

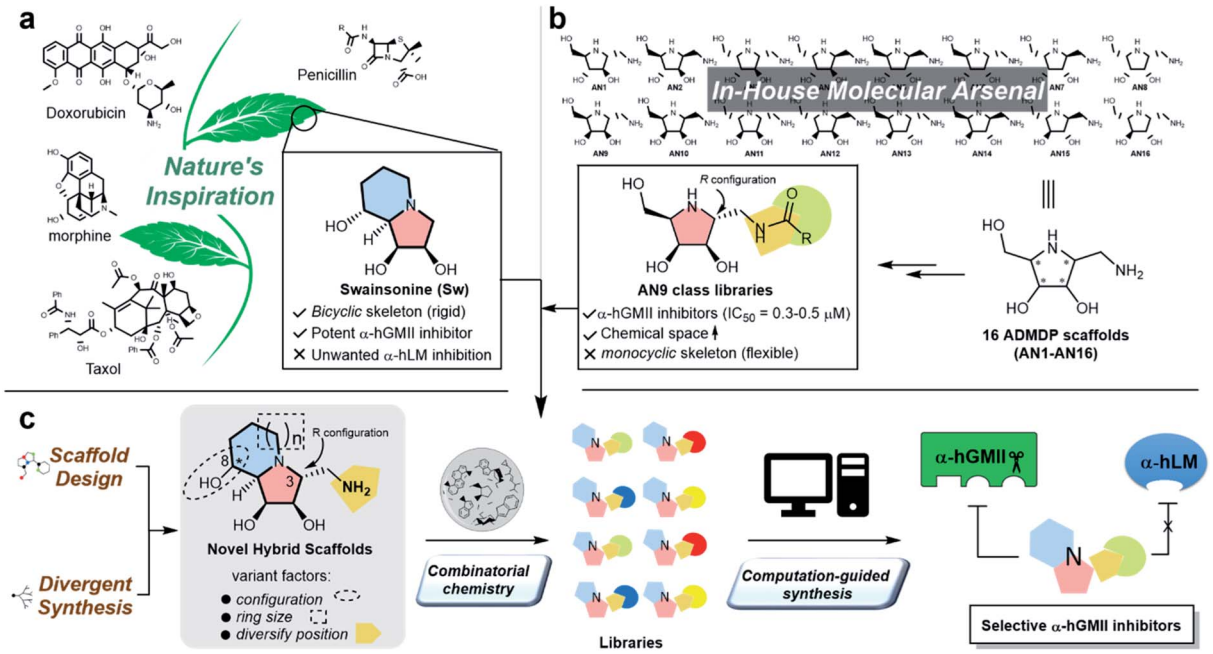

Fig. 1 The natural product-inspired discovery of new selective α-hGMII inhibitors. Inspired by (a) sw and (b) AN9-type molecules from our in-house molecular arsenal to (c) design and synthesize novel scaffolds with core-, configuration- and substituent diversity in a divergent manner for exploration of selective α-hGMII inhibitors assisted by combinatorial chemistry and computation-guided synthesis.

The resulting inhibitors were assessed for their *in vitro N*-glycan modulation, anti-hepatocellular carcinoma (HCC) activity, cell migration and invasion studies, and *in vivo* anti-HCC activity.

Results and discussion

General chemistry strategy and new molecular scaffold design

Inspired by the skeletons of sw and AN9, a new bicyclic scaffold bearing a C3 aminomethyl group with the *R* configuration (Fig. 1c) was adopted as the basic structure for the development of a novel and selective α-hGMII inhibitor. A bicyclic-based scaffold was selected due to its conformational constraints, which were anticipated to decrease internal molecular rotations and hence improve the binding potency or selectivity.[21] Scaffolds incorporating both C8 epimers and alternately sized rings were prepared and assessed for their inhibitory selectivity. To efficiently synthesize molecules for testing, a divergent synthetic approach incorporating several common intermediates was planned.[22] The C3 aminomethyl moiety of these scaffolds was anticipated to allow rapid substituent diversity *via* the amide or (thio)urea formation, and conjugation with a structurally diverse carboxylic acid or isocyanate library collection, increasing the chemical space for further enzyme inhibition and selectivity studies. Further structural modifications were guided by computational analysis and docking studies to efficiently create the advanced α-hGMII inhibitors (Fig. 1c).

Preparation and bioevaluation of scaffolds 8a, 8b, 10a, and 10b

Our synthesis of desired scaffolds **8a**, **8b**, **10a**, and **10b** commenced with cyclic nitrone **1**, prepared from L-ribose according to previous reports (Fig. 2a).[19,23] Selective nucleophilic addition of TMSCN to **1** followed by (i) our previously reported, one-pot N–O and nitrile reduction in the presence of Boc_2O using RANEY® Ni/H_2,[19] (ii) selective deprotection of the trityl group under mild acidic conditions (formic acid),[24] and (iii) Dess–Martin periodinane (DMP) oxidation led to aldehyde **3** (52% yield over 4 steps). Notably, **3** could be prepared on a multigram scale (>10 g), qualifying it as a common intermediate for our divergent synthetic application. Aldehyde **3** was reacted with AllylMgBr to afford the homoallylic alcohol **4a**.[20] The high diastereoselectivity of this transformation can be explained using the Felkin–Ahn model;[25] the stereochemistry of **4a** was confirmed by X-ray crystallographic analysis (Fig. 2b).

Initial attempts to prepare scaffold **8a** from **4a** by either (i) S_N2-type cyclization,[20] or (ii) reductive amination/cyclization resulted in intractable mixtures of products containing only very low yields of **8a** (Fig. 2b and ESI S1†). Accordingly, we redesigned the synthetic route (Fig. 2c). Following the similar conversion from **3** to **4a**, nucleophilic addition of 3-butenylMgBr to **3** gave **6a** as a single isomer (78%). Removal of the two *N*-Boc groups of **6a** using $ZnBr_2$ [26,30] followed by *N*-Cbz protection furnished bis-*N*-Cbz **7a** (69% over 2 steps). Lemieux–Johnson oxidation of **7a**[27] followed by reductive amination (H_2, Pd/C) and acetonide deprotection resulted in an excellent yield of the first scaffold **8a** (80% over 3 steps), the configuration of which was confirmed by 2D NOESY analysis (Fig. 2c).

Our attention then turned to the synthesis of scaffold **8b**, the C8-epimer of **8a** (Fig. 2d). Intermediate **6a** was reacted with Tf_2O to generate cyclic carbamate **6b** (incorporating the appropriately inverted chiral center) in 73% yield.[28] The stereochemistry of **6b** was determined by 2D NOESY NMR analysis. Hydrolysis of **6b**

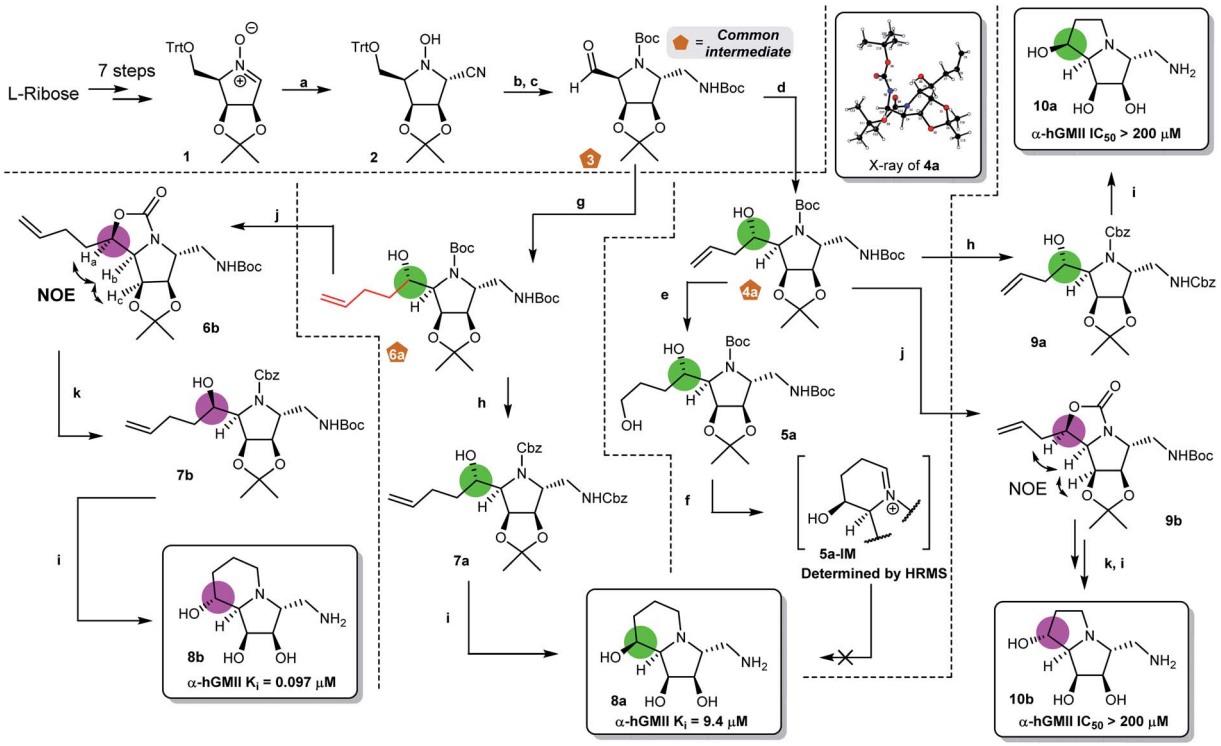

Fig. 2 Pathways for synthesis of target scaffolds **8a**, **8b**, **10a** and **10b**. Reagents and conditions: (a) TMSCN, MeOH, 50 °C, 2 h, 90%. (b) (1) RANEY® Ni, H_2, Boc_2O, MeOH, 8 h, rt, 74%; (2) HCOOH, Et_2O, rt, 2 h, 78%. (c) DMP, CH_2Cl_2, rt, 2 h, 99%. (d) AllylMgCl, THF, 0 °C to rt, 1 h, 64%. (e) BH_3-THF, THF, rt, 1 h, then, $NaOH_{(aq)}$, H_2O_2, rt, 1 h, 75%. (f) (1) DMP (1.1 eq.), CH_2Cl_2, rt, 2 h. (2) TFA, CH_2Cl_2, 0 °C, 1 h. (3) Pd/C, H_2, MeOH, rt, o.n. (g) 3-butenylMgBr, THF, 0 °C to rt, 1 h, 78%. (h) (1) $ZnBr_2$, CH_2Cl_2, rt, 12 h; (2) CbzCl, $NaHCO_{3(aq)}$, THF, rt, 3 h, 69% (**7a**) and 76% (**9a**) over 2 steps. (i) (1) OsO_4, $NaIO_4$, 2,6-lutidine, dioxane/H_2O, rt, 8 h; (2) Pd/C, H_2, MeOH, rt, o.n. (3) HCl, MeOH, rt, 8 h, 80% (**8a**), 90% (**8b**), 84% (**10a**) and 78% (**10b**) over 3 steps. (j) Tf_2O, py, CH_2Cl_2, 0 °C to rt, 3 h, 73% (**6b**) and 75% (**9b**). (k) (1) LiOH, EtOH, H_2O, 90 °C, 12 h; (2) CbzCl, $NaHCO_{3(aq)}$, THF, rt, 3 h, 69% (**7b**) and 73% (**S17**) over 2 steps. HRMS refers to high resolution mass.

followed by *N*-Cbz protection gave alcohol **7b** in 69% yield over 2 steps. Similarly, following the sequence of transformations from **7a** to **8a**, the second desired scaffold **8b** was synthesized from **7b** in 90% over 3 steps.

The preparation of the two ring-contracted scaffolds **10a** and **10b** is depicted in Fig. 2e. Compound **4a** was subjected to similar conditions as that for **6a**, and then two new scaffolds **10a** (64% over 5 steps) and **10b** (43% over 6 steps) were obtained. Notably, **10a** was also obtained from **4a** using our established protocol *via* the S_N2 type cyclization.[20] Chemically, we successfully developed synthetic routes to prepare common intermediates **3**, **4a**, and **6a**, which play a key role in building our desired scaffolds.

With four scaffolds **8a**, **8b**, **10a**, and **10b** in hand, their inhibitory activity against α-hGMII was evaluated. As shown in Fig. 2, **8a** was less active (IC_{50} = 48 μM) compared to **8b** (IC_{50} = 0.65 μM), but both **8a** and **8b** (5-6 ring fused analogues) were found to have better activities compared to their ring-contracted analogues **10a** and **10b** (5-5 fused analogues), which showed nearly no α-hGMII inhibition (IC_{50} > 200 μM). These findings suggested that the ring size of the second ring and the orientation of the C8 hydroxyl group significantly influence the inhibitory potency. Based on these results and the incorporation of a pendent amino methylene moiety considered suitable for structural diversity, **8b** was selected for further development.

Discovery of selective α-hGMII inhibitors *via* NPICC and CGS

Scaffold **8b** was coupled with a random selection of 96 iso(thio) cyanates to generate the corresponding (thio)urea derivatives *via* combinatorial parallel synthesis (ESI Fig. S2†).[29] After 24 h, **8b** was consumed and formation of the corresponding product was monitored by TLC or MS. The reaction was quenched by adding an aqueous buffer (see ESI methods†). The products were directly evaluated without further purification in an enzyme-based assay, as previously reported.[15] Only **8b-1** was found to exhibit a high relative inhibition ratio (RIR) of around 3.7 (the RIR values of most analogues including sw and scaffold **8b** were in the range of 0.36 to 1.06). Compound **8b-1** was therefore considered to be a promising hit worthy of further investigation (ESI Fig. S3†).

After re-synthesis of **8b-1** and its truncated form **8b-2** (for comparison), their inhibition constant (K_i) and selectivity were examined (Fig. 3b and S5 ESI†). The selectivity index (SI) of **8b-1**, **8b-2**, scaffold **8b**, and sw was 13.5, 3.1, 3.7, and 4.6, respectively. The α-hGMII inhibitory activities of **8b-1** (K_i = 0.35 μM, competitive) and **8b-2** (K_i = 0.2 μM, competitive) were similar, indicating that the 4-hexylcyclohexyl moiety of **8b-1** does not significantly contribute to its potency. In contrast, **8b-1** (K_i = 4.72 μM, competitive) was 8-fold less potent than **8b-2** (K_i = 0.61 μM, competitive) against α-hLM; presumably binding of the

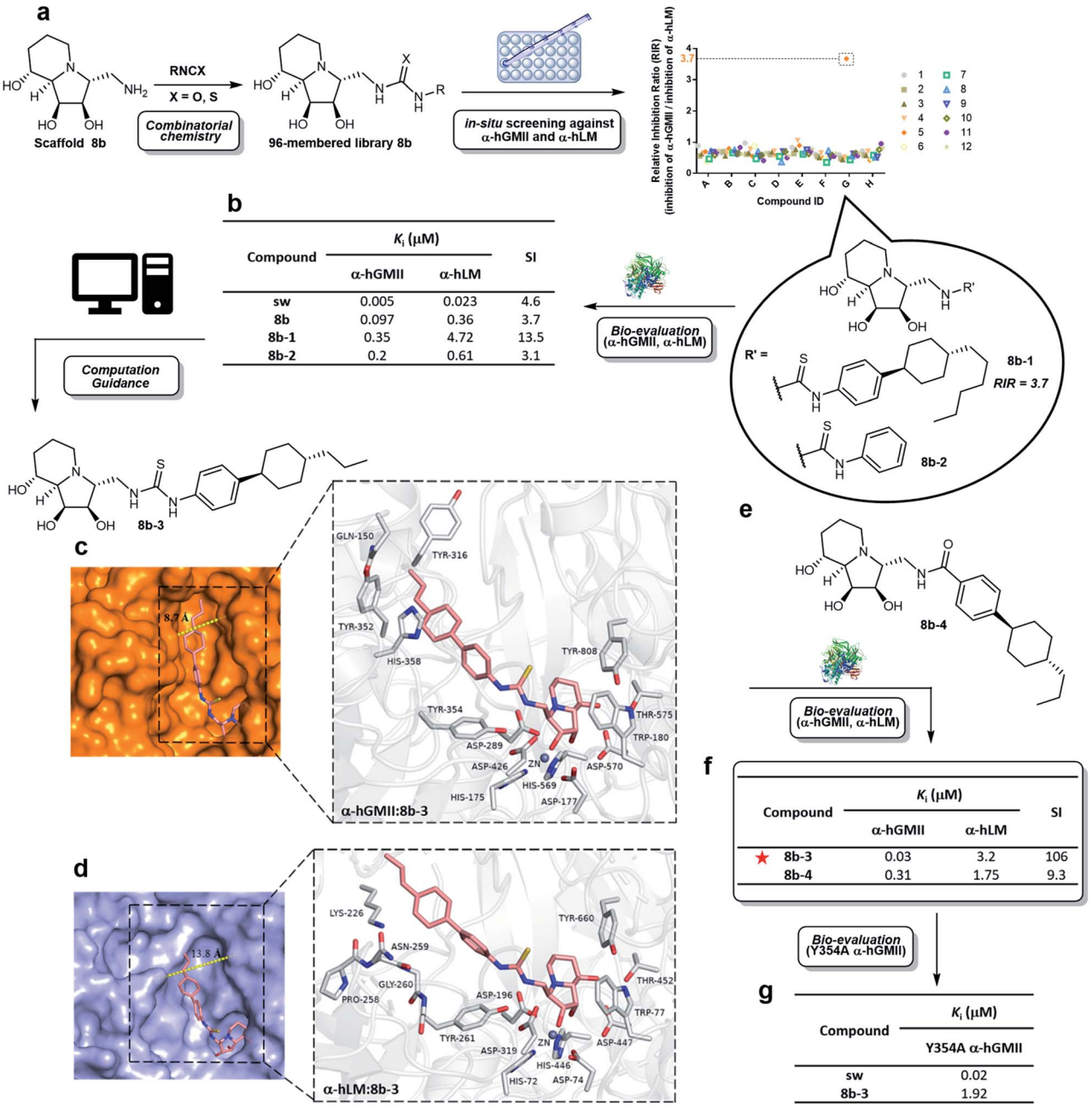

Fig. 3 Synthesis and evaluation of a compound library. (a) Parallel synthesis of library **8b** followed by *in situ* enzyme-based inhibition evaluation against α-hGMII and α-hLM to discover potentially selective α-hGMII inhibitors. (b) Table of α-hLM, α-hGMII inhibition data of sw, **8b**, **8b-1** and **8b-2**. Computational modeling of the complex between (c) α-hGMII and **8b-3** and (d) α-hLM and **8b-3**. (e) Molecular structure of **8b-4**. (f) Table of α-hLM, α-hGMII inhibition data of **8b-3** and **8b-4**. (g) Table of Y354A α-hGMII inhibition data of sw and **8b-3**. Assays were conducted using Man-α-4MU as the substrate (5 mM for wild-type α-hGMII; 2.5 mM for α-hLM and Y354A α-hGMII) and are described in the ESI.† The K_m of α-hLM, α-hGMII and Y354A α-hGMII toward 4MU-α-Man is 0.56, 1.22 and 0.63 mM, respectively (ESI Fig. S4†). RIR: Relative inhibition ratio = inhibition percentage against α-hGMII/inhibition percentage against α-hLM at certain concentrations; K_i: inhibition constant; SI: selectivity index = [(α-hLM K_i)/(α-hGMII K_i)]; data are the mean of three determinations.

hydrophobic substituent of **8b-1** was not favorable in the α-hLM binding pocket, but its attenuation of the α-hLM enzyme activity increased the SI value (**8b-1** *vs.* **8b-2**). Therefore, **8b-1** was selected for further development.

To date, no structure of α-hLM and α-hGMII is available. In contrast, both α-dGMII and α-bLM display high sequence identity with their corresponding α-hGMII and α-hLM, respectively, (ESI Fig. S6†) and their crystal structures are accessible, allowing us to apply them as the 3D templates to build the human enzyme structures for molecular docking (ESI Fig. S7†).[18,30] In our study, the residues of the indolizidine-binding pocket in both enzymes were highly conserved, and

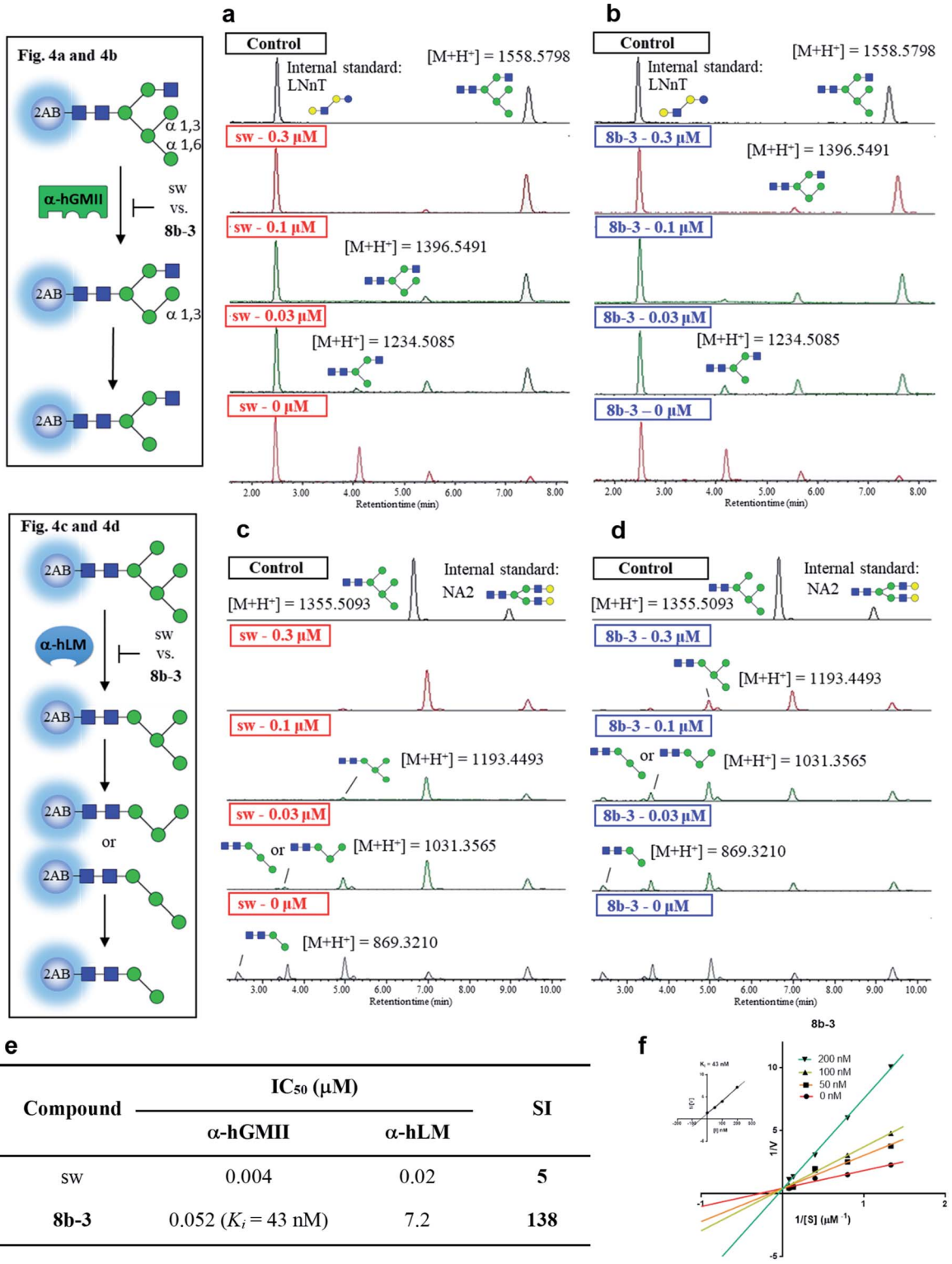

e

Compound	IC_{50} (μM)		SI
	α-hGMII	α-hLM	
sw	0.004	0.02	**5**
8b-3	0.052 (K_i = 43 nM)	7.2	**138**

Fig. 4 Study of selectivity index of **8b-3** for α-hLM *vs.* α-hGMII inhibition with oligosaccharides as a natural substrate. The α-hGMII and the glycan substrate ($GlcNAcMan_5GlcNAc_2$-2AB, also called GlcNAcMan5-2AB) were treated with (a) sw and (b) **8b-3** in a dose-dependent manner (0, 0.3, 0.1, 0.03 μM) for 24 h at 37 °C using Gal-β-1,4-GlcNAc-β-1,3-Gal-β-1,4-Glc-2AB (LNnT-2AB) as the internal standard based on the peak area ratio to determine the inhibition activity. The α-hLM and the glycan substrate ($Man_5GlcNAc_2$-2AB, also called Man5-2AB) were treated with (c) sw and (d) **8b-3** in a dose-dependent manner (0, 0.3, 0.1, 0.03 μM) for 24 h at 37 °C using $(Gal\text{-}GlcNAc)_2Man_3(GlcNAc)_2$-2AB (NA2-2AB) as the internal standard based on the peak area ratio to determine the inhibition activity. (e) Glycan based α-hLM and α-hGMII inhibition data (ESI Fig. S11†), and selectivity index (SI) of sw and **8b-3**. (f) Lineweaver–Burk plot for K_i determination of inhibitor **8b-3** against α-hGMII. Assays were conducted as described in the ESI.† IC_{50}: half-maximal inhibitory concentration; SI: selectivity index = [(α-hLM IC_{50})/(α-hGMII IC_{50})]; data are the mean of three determinations.

the binding modes of the indolizidine moiety of sw and **8b-1** were similar, implying that the selectivity of **8b-1** is mainly due to its substituents. The thiourea and phenyl moieties of **8b-1** were found to create two new hydrogen bonding interactions and a π–π interaction with Tyr 354; the 4-hexylcyclohexyl moiety of **8b-1** might undergo extra sigma–π interactions with Tyr 352 and His 358, and hydrophobic interactions with the nonpolar side chain of Gln 150 and Tyr 316 of α-hGMII (ESI Fig. S8a†). However, the 4-hexylcyclohexyl moiety of **8b-1** did not show sigma–π or hydrophobic interaction in the α-hLM model. Furthermore, the active site cleft of α-hLM is much wider than that of α-hGMII (13.8 Å *vs.* 8.7 Å), indicating that binding between **8b-1** and α-hLM is disfavored since the hydrophobic moiety of **8b-1** precludes its binding to the hydrophilic region in α-hLM (ESI Fig. S8b†).

To assist in the design of **8b-1** derivatives, several molecules were proposed and their α-hGMII binding energies were calculated (ESI Table S1†). Among them, **8b-3** incorporating a 4-propylcyclohexyl moiety was selected for investigations and its molecular models with α-hGMII and α-hLM were built (Fig. 3c and d). The binding mode of **8b-3** with α-hGMII showed that the 4-propylcyclohexyl moiety could undergo more sigma–π interactions with His 358 and Tyr 352 and offers less steric hindrance with protein residues, compared to **8b-1** bearing the longer hexyl chain (Fig. 3c and ESI S8c†). In contrast, the hydrophobicity of **8b-3**, like **8b-1**, disfavored its binding with α-hLM (Fig. 3d). Thus, we were hopeful that **8b-3** would be a potent and selective α-hGMII inhibitor.

Thiourea **8b-3** was synthesized, along with amide **8b-4** (for comparison purposes, Fig. 3e). Results showed that **8b-3** exhibited nanomolar potency against α-hGMII (K_i = 0.03 μM, competitive), a tenfold increase of α-hGMII inhibition compared to **8b-1**, with the SI up to 106 (Fig. 3f, ESI S5†). As predicted, **8b-4** was much less potent than **8b-3** against α-hGMII and much less selective (SI value = 9.3), indicating that the thiourea linkage is better than the amide moiety. We also undertook a mutagenesis study; the activity of **8b-3** against Y354A α-hGMII was reduced by about 64-fold (K_i = 1.92 μM, competitive) compared to wild-type α-hGMII, suggesting that the phenyl ring of **8b-3** and the aromatic residue of Tyr 354 in α-hGMII significantly interact (π–π interactions) (Fig. 3g, S5 ESI†). In contrast, the K_i values of sw for Y354A and wild-type were similar, presumably because sw lacks substituents.

Studies of inhibitors with natural substrate-like oligosaccharides as enzyme substrates

In the preceding bioassays, the fluorogenic Man-α-4MU was selected as an easy and accessible substrate for both enzymes. However, the natural substrates of both enzymes are quite structurally different. Accordingly, we sought to prepare glycan bio-substrates more closely resembling those found *in vivo*, to further investigate the inhibition potency and selectivity of qualified inhibitors such as **8b-3** in an *in vitro* enzyme activity platform. In our UPLC-based assay platform, fluorescence labelling of glycan substrates with 2-aminobenzamide (2AB) was required to increase the signal sensitivity to easily monitor the enzyme activity or inhibitor activity through the peak area ratio of the remaining substrate to the internal standard.[31] Based on our design, $GlcNAcMan_5GlcNAc_2$-2AB and $Man_5GlcNAc_2$-2AB[32] were chosen as the substrate of α-hGMII and α-hLM, respectively. Gal-β-1,4-GlcNAc-β-1,3-Gal-β-1,4-Glc-2AB (LNnT-2AB) and $(Gal\text{-}GlcNAc)_2Man_3(GlcNAc)_2$-2AB (NA2-2AB) were chosen as the internal standard for the α-hGMII assay and α-hLM assay, respectively. Notably, $GlcNAcMan_5GlcNAc_2$-2AB was prepared from $Man_5GlcNAc$-2AB by the addition of a β-1,2-*N*-acetylglucosamine *via* the GnT-I catalyzed enzymatic synthesis (ESI Fig. S9†).[33] As shown in UPLC spectra under varied conditions (Fig. 4 and S10, ESI†), $Man_5GlcNAc_2$-2AB was hydrolyzed by α-hLM into possible products including Man_4-, Man_3-and Man_2-$GlcNAc_2$-2AB.[34] Likewise, $GlcNAcMan_5GlcNAc_2$-2AB was digested by α-hGMII into two possible products, $GlcNAcMan_4GlcNAc_2$-2AB and $GlcNAcMan_3GlcNAc_2$-2AB.[8,9]

Both **8b-3** and sw exhibited dose-dependent inhibition (ESI Fig. S11†). Importantly, the SI of **8b-3** was around 138, while sw showed a much poorer selectivity (SI = 5) (Fig. 4e). Furthermore, the enzyme kinetics showed that **8b-3** is a potent competitive inhibitor (K_i = 43 nM) against α-hGMII (Fig. 4e and f). This reassuring finding indicates that the inhibition behavior of **8b-3** is similar in two assay systems without substrate dependence. Through this unprecedented inhibition and selectivity study, our exciting results established that **8b-3** is not only an effective α-hGMII inhibitor but also a selective inhibitor, worthy of further biochemistry experiments for anticancer drug discovery.

Modulation of cellular *N*-glycans with 8b-3

Modulation of *N*-glycans with **8b-3** was explored by monitoring the lysosomal catabolic and biosynthetic pathways in cell culture (Fig. 5a). To expedite the analysis, LC-MS was extensively utilized instead of the conventional TLC methods reported by Dr Winchester.[35,36]

Accumulation of $Man_{2\text{-}9}GlcNAc$ in human fibroblasts caused by mannosidase inhibitors

Based on the *N*-glycan catabolism in the lysosomes, the biomarkers of α-LM inhibition are the mannose-rich oligosaccharides possessing only one GlcNAc ($Man_{2\text{-}9}GlcNAc$) at the reducing end after the lysosomal chitobiase specifically cleaving glycoprotein carbohydrate chains, allowing us to easily monitor the specific lysosomal *N*-glycans by LC-MS without complex pretreatments like enzymatic digestion.[37] As shown in Fig. 5b and c, as expected, after 24 h treatment with sw, the relative intensity of overall $Man_{2\text{-}9}GlcNAc$ increased by about 5-fold compared to the control group indicating that the $Man_{2\text{-}9}GlcNAc$ substrate obviously accumulated caused by α-LM inhibition. In contrast, the oligomannosidic accumulation caused by **8b-3** is milder than that caused by sw (about 30% decrease at 20 μM), consistent with the results of the α-hLM inhibition study in Fig. 3 and 4 (ESI Table S2†). This finding suggests that its clinical use may be associated with fewer side effects resulting from the accumulation of undegraded oligosaccharides in lysosome compared to sw.

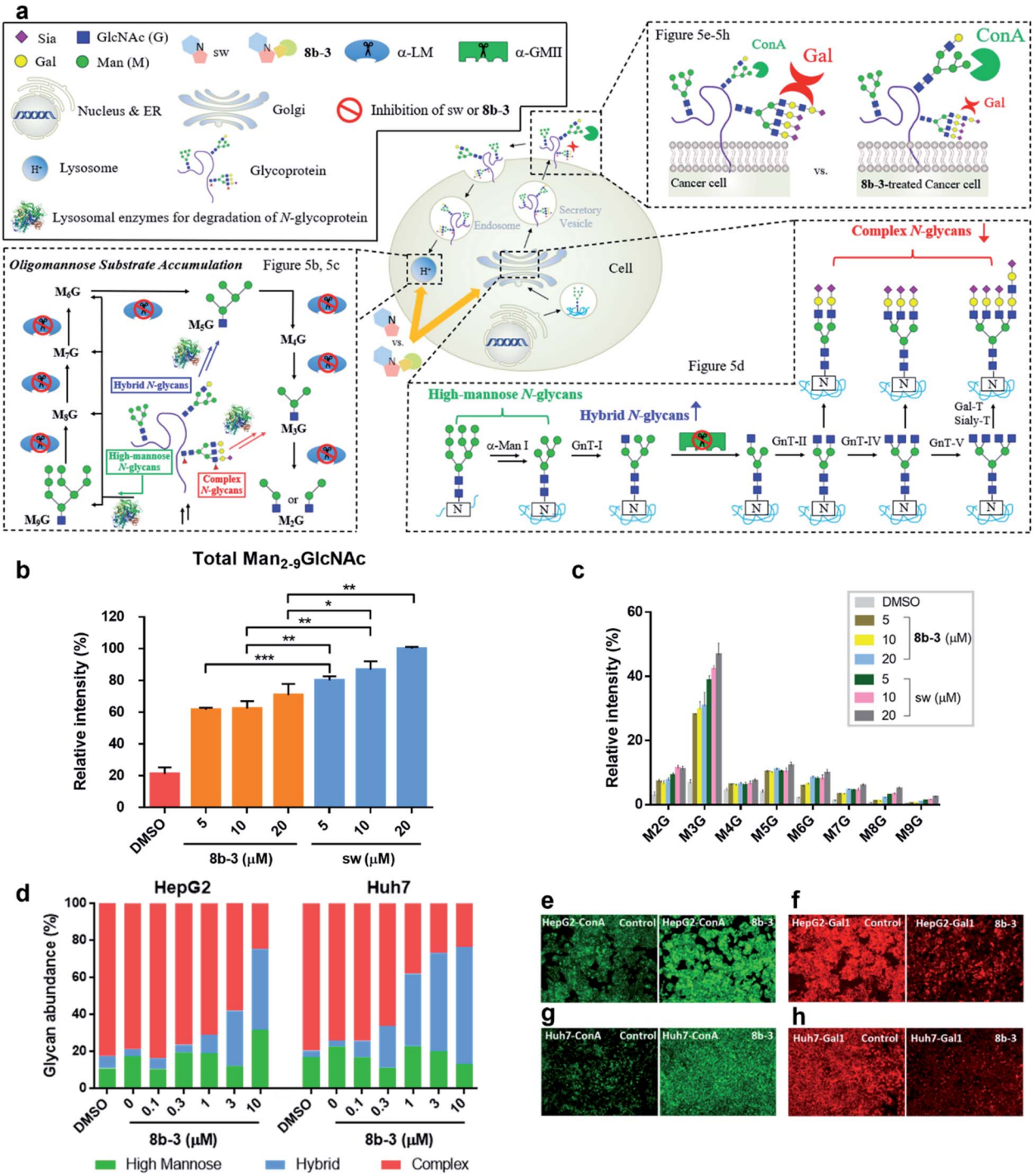

Fig. 5 Cellular effect of sw and **8b-3** in Golgi and lysosome. (a) Schematic representation of the effect of inhibition of sw and **8b-3** against α-LM and α-GMII in the cell. (b) Histogram showing LC-MS analysis of total accumulated oligomannose substrate $Man_{2\text{-}9}GlcNAc(M_{2\text{-}9}G)$ and (c) accumulation of $Man_{2\text{-}9}GlcNAc$ in human normal fibroblast (08C0015) in the presence of mannosidase inhibitors sw or **8b-3** from 5 to 20 μM compared to the control culture (accumulated substrate in the cell treated with 20 μM sw is denoted as 100%). (d) Relative *N*-glycan abundance of HepG2 and Huh7 treated with **8b-3** in a dose-dependent manner compared to the control culture was analyzed by LC-MS. Mean values of glycan abundance (%) are shown as means of two independent experiments. Microscope images of untreated and **8b-3**-treated HepG2 cells stained with (e) FITC conjugated concanavalin (ConA-FITC, green) and (f) Alexa Fluor 555 conjugated Galectin 1 (Gal1-555, red), and Huh7 cells stained with (g) ConA-FITC and (h) Gal1-555. $^{*}P < 0.05$, $^{**}P < 0.01$, $^{***}P < 0.001$, $P < 0.05$ is considered statistically significant.

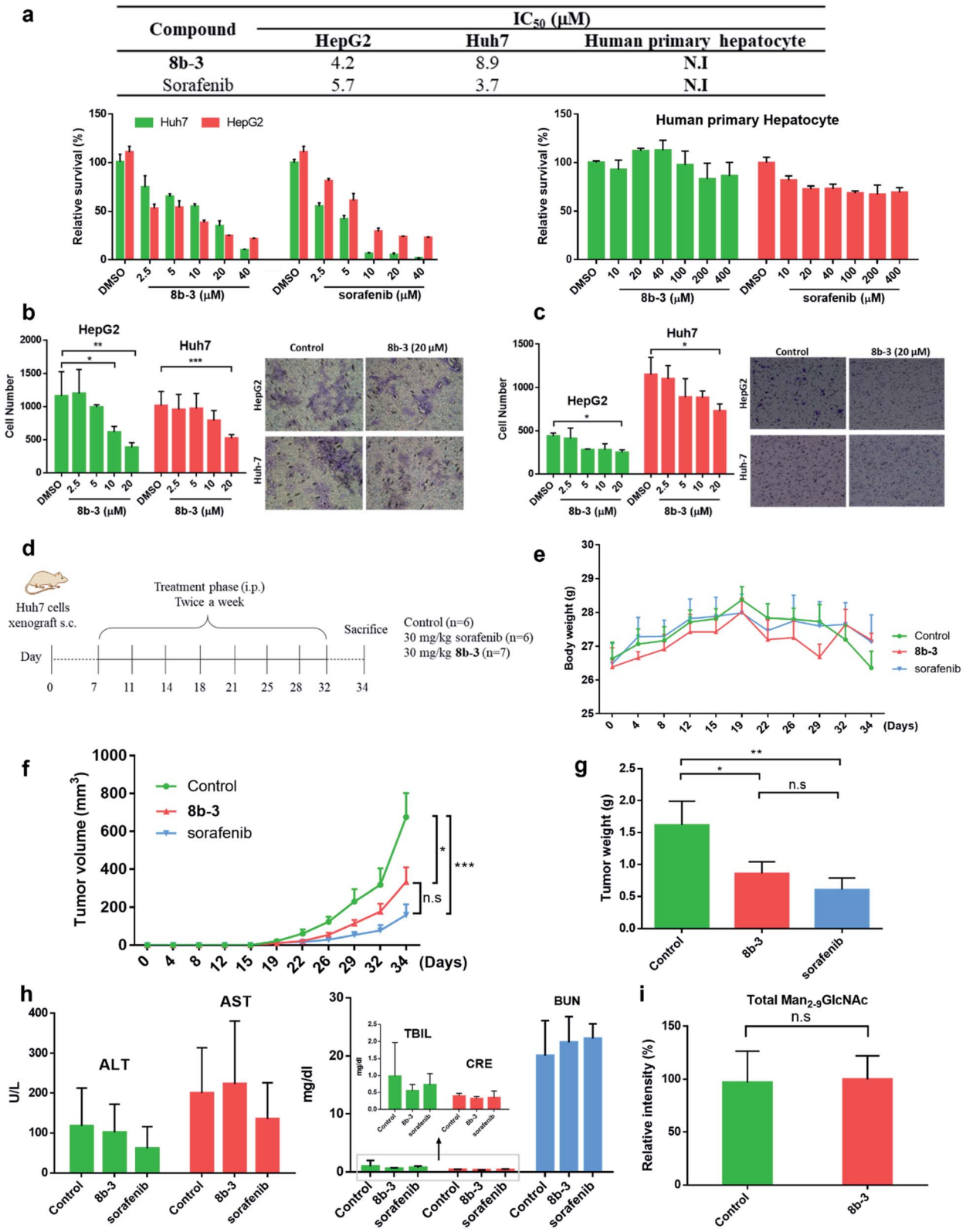

Fig. 6 Iminosugar **8b-3** inhibits HCC *in vitro* and *in vivo* compared with sorafenib. (a) Table of cell viability data (MTT) of HepG2, Huh7, and human primary hepatocyte treated with **8b-3** and sorafenib for 72 h. The assay was conducted as described in the ESI.† NI: no inhibition. IC_{50}: half-maximal inhibitory concentration; data are the mean of three determinations. The effects of **8b-3** on cell (b) migration and (c) invasion of HepG2 and Huh7 cells were tested by the Transwell assay. (d) Animal experimental schedule. (e) The bodyweights of mice were monitored. (f) The tumor volume (mm^3) was recorded. (g) The final weights of the subcutaneous xenograft tumors. Assessment of the hepatorenal toxicity of the drugs by analyzing (h) the aspartate aminotransferase (AST), alanine aminotransferase (ALT), total bilirubin (TBIL), creatinine (CRE), and blood urea nitrogen (BUN) levels. (i) Histogram showing the LC-MS analysis of total accumulated oligomannose substrate ($Man_{2-9}GlcNAc$) in the serum sample from control and **8b-3** treated mice (accumulated substrate in the serum from mice treated with **8b-3** is denoted as 100%). *P < 0.05, **P < 0.01, ***P < 0.001, P < 0.05 is considered statistically significant, n. s. refers to not significant.

Treatment of 8b-3 to alter the *N*-glycosylation of liver cancer cells

To understand the effect of α-hGMII inhibitor **8b-3** on the pattern of cellular *N*-glycosylation, HepG2 and Huh7 cells were treated with **8b-3** at varying concentrations (0–10 μM) and, after 72 h, their glycan profiles analyzed by LC-MS (see ESI methods†).[38] As shown in Fig. 5d, the *N*-glycans of untreated HepG2 and Huh7 were mostly complex-type glycans incorporating sialic acids and fucoses, with relatively few high-mannose or hybrid-type glycans (ESI Table S3 and 4†). In contrast, treatment with **8b-3** shifted the *N*-glycopatterns from complex- to hybrid-type glycans in a dose dependent manner (Fig. 5d).

Subsequently, the cell surface binding of fluorogenic lectins was investigated in the presence or absence of **8b-3** (Fig. 5e–h). Binding of FITC-labeled concanavalin A (ConA-FITC), a mannose binding lectin, markedly increased on these two cells treated with **8b-3** (10 μM) for 48 h.[39] This indicated that more mannose-containing glycans (both high-mannose type and newly abundant hybrid type *N*-glycans) were detected on the cell surface, upregulated by α-hGMII inhibition of **8b-3** (Fig. 5e and g). Likewise, after treatment with **8b-3**, binding of fluorogenic galectin-1 (Gal1-555) substantially decreased because of the lower abundance of β-galactose containing moieties such as *N*-acetyl lactosamine which are normally abundant in complex type *N*-glycans (Fig. 5f and h).[40,41] Thus, inhibition of α-hGMII with **8b-3** altered the *N*-linked glycosylation process, demonstrating that both lectin binding results are complementary.

Taken together, we established that **8b-3** is a potent α-hGMII inhibitor capable of reducing the biosynthesis of complex type *N*-glycans, and, unlike sw, does not significantly impede α-hLM bioactivity which can result in the storage of oligomannose glycans in the lysosomes. These very promising outcomes encouraged us to subject **8b-3** to further anticancer activity studies and *in vivo* study of small molecule-induced storage of oligomannose glycans in serum.

Studying the *in vitro* and *in vivo* anticancer activity of 8b-3

Finally, the cytotoxicity of **8b-3** towards HCC cells including HepG2 and Huh7 cells was examined using sorafenib, a first-line therapy for advanced HCC, as a control.[42] Interestingly, both **8b-3** and sorafenib exhibited low micromolar inhibition and anti-proliferation activities (Fig. 6a). For testing the potentially toxic side effects of **8b-3**, the viability of primary human hepatocytes (HPH) was primarily evaluated and the MTT results revealed that **8b-3** has little cytotoxicity, even up to 400 μM. Significantly, **8b-3** suppressed cell migration and invasion of both HCC cell lines in a dose-dependent manner (Fig. 6b and c). α-hGMII inhibition causing a reduction in the synthesis of complex type glycans is consistent with these results.

Next, the *in vivo* anticancer activity of **8b-3** was studied. In a typical procedure, xenograft tumors were generated by implanting Huh7 cells (5×10^6) subcutaneously into the left and right flanks of NOD-SCID mice. Starting on the 7th day after the inoculation of Huh7 cells, the mice were individually injected with either **8b-3** or sorafenib intraperitoneally (ip.) at a dose of 30 mg kg^{-1} and twice a week for 34 days (Fig. 6d). During treatment, neither mice injected with **8b-3** nor sorafenib exhibited signs of harm or decreased body weight (Fig. 6e). Our animal results (Fig. 6f and g) showed a significant reduction in tumor growth when administered with **8b-3** and sorafenib ($P < 0.05$) compared to the control. In addition, no serious side effects including hepatotoxicity and nephrotoxicity were observed (Fig. 6h and ESI Table S5†). Importantly, no significant accumulation of oligomannose glycans was detected in the serum of **8b-3**-treated mice compared to the control (Fig. 6i and ESI Table S6†). These promising *in vivo* results demonstrate that **8b-3** is a selective α-hGMII inhibitor exhibiting anti-tumor activity against HCC cells, without affecting the storage of oligomannoses in the serum.

Conclusions

Inhibition of α-hGMII is known to alter *N*-glycan distribution patterns, suppressing cancer growth and metastasis, but most known inhibitors are poorly selective for α-hGMII over α-hLM (inhibition of which leads to abnormal storage of oligomannoses), limiting their further therapeutic potential. In this study, we successfully developed a new class of α-hGMII inhibitor **8b-3**, with nanomolar potency against α-hGMII but little activity against α-hLM. This discovery was greatly accelerated by the exploration of new divergent synthetic approaches to build common intermediates and desired scaffolds, as well as adoption of NPICC and CGS.

Notably, no toxic side-effects of **8b-3** toward HPH were observed, and the *in vivo* anticancer study showed that **8b-3** is an anti-HCC agent. No abnormal storage of oligomannoses was detected in the serum compared with normal controls. Moreover, our preliminary results showed that **8b-3** has similar anti-HCC potencies with the FDA approved drug sorafenib, and it is worthy of future systematic studies toward HCC or other tumors, as well as immunomodulatory studies.[7,43–45]

In the course of this work, **8b-3** was evaluated in a series of cell-based assay platforms. Notably, this is the first report describing the use of natural substrate-like oligosaccharides to characterize the potency and selectivity of inhibitors against α-hGMII and α-hLM in a UPLC study, as well as how to use LC-MS to analyze the accumulation of oligomannose glycans ($Man_{2\text{-}9}$-GlcNAc) in treated cells.

Finally, our synthetic chemistry strategy for efficiently developing selective inhibitors should be readily applicable to other targets or sugar processing enzymes. Additional studies are ongoing, and the results will be reported in due course.

Data availability

Experimental and computational data associated with this work are provided in the accompanying ESI†.

Author contributions

W.-C. C. and W.-A. C. designed the experiments. W.-A. C. performed most of the experiments. W.-A. C. synthesized

compounds with support from C.-W. C. W.-A. C. performed molecular libraries, *in situ* screening, compounds' resynthesis and enzyme kinetic studies. T.-J. R. C. provided α-hGMII and α-hLM. Y.-T. W. and W.-A. C. performed SAR and computational studies. Y.-H. C. and T.-L. H. performed enzyme kinetic studies using oligosaccharides as the natural substrate. W.-A. C. and T.-L. H. performed cell-based *N*-glycan profiling and oligomannose accumulation analysis by LC-MS assisted by C.-H. C. and J.-L. L. W.-A. C. performed fluorescence imaging. W.-A. C, C.-Y. H. and P.-F. H. performed cellular viability, migration and invasion assays. C.-N. S. designed *in vivo* studies, and C.-Y. H. and P.-F. H. performed the experiments. W.-A. C. wrote the manuscript and compiled the ESI.† T.-J. R. C., Y.-T. W., T.-L. H., J.-L. L. and C.-N. S. provided scientific input. W.-A. C. and W.-C. C analyzed the data, discussed the results, and contributed to the editing of the manuscript. W.-C. C. and C.-N. S. supervised the entire project.

Conflicts of interest

There are no conflicts to declare.

Acknowledgements

We thank Academia Sinica and the Ministry of Science and Technology for financial support and the Core Facilities of Translational Medicine of BioTReC (National Biotechnology Research Park, Academia Sinica, Taiwan) for the technical support and data analysis.

Notes and references

1 K. Ohtsubo and J. D. Marth, *Cell*, 2006, **126**, 855–867.
2 G. W. Hart and R. J. Copeland, *Cell*, 2010, **143**, 672–676.
3 S. S. Pinho and C. A. Reis, *Nat. Rev. Cancer*, 2015, **15**, 540–555.
4 C. Reily, T. J. Stewart, M. B. Renfrow and J. Novak, *Nat. Rev. Nephrol.*, 2019, **15**, 346–366.
5 M. M. Fuster and J. D. Esko, *Nat. Rev. Cancer*, 2005, **5**, 526–542.
6 J. M. H. van den Elsen, D. A. Kuntz and D. R. Rose, *EMBO J.*, 2001, **20**, 3008–3017.
7 P. E. Goss, M. A. Baker, J. P. Carver and J. W. Dennis, *Clin. Cancer Res.*, 1995, **1**, 935.
8 N. Shah, D. A. Kuntz and D. R. Rose, *Proc. Natl. Acad. Sci. U. S. A.*, 2008, **105**, 9570.
9 D. R. Rose, *Curr. Opin. Struct. Biol.*, 2012, **22**, 558–562.
10 S. R. Stowell, T. Ju and R. D. Cummings, *Annu. Rev. Phytopathol.*, 2015, **10**, 473–510.
11 D. A. Kuntz, C. A. Tarling, S. G. Withers and D. R. Rose, *Biochemistry*, 2008, **47**, 10058–10068.
12 Z. Armstrong, C.-L. Kuo, D. Lahav, B. Liu, R. Johnson, T. J. M. Beenakker, C. de Boer, C.-S. Wong, E. R. van Rijssel, M. F. Debets, B. I. Florea, C. Hissink, R. G. Boot, P. P. Geurink, H. Ovaa, M. van der Stelt, G. M. van der Marel, J. D. C. Codée, J. M. F. G. Aerts, L. Wu, H. S. Overkleeft and G. J. Davies, *J. Am. Chem. Soc.*, 2020, **142**, 13021–13029.
13 T. Fujita, H. Nagasawa, Y. Uto, T. Hashimoto, Y. Asakawa and H. Hori, *Org. Lett.*, 2004, **6**, 827–830.
14 D. A. Kuntz, S. Nakayama, K. Shea, H. Hori, Y. Uto, H. Nagasawa and D. R. Rose, *ChemBioChem*, 2010, **11**, 673–680.
15 T.-J. R. Cheng, T.-H. Chan, E.-L. Tsou, S.-Y. Chang, W.-Y. Yun, P.-J. Yang, Y.-T. Wu and W.-C. Cheng, *Chem.–Asian J.*, 2013, **8**, 2600–2604.
16 S. Šesták, M. Bella, T. Klunda, S. Gurská, P. Džubák, F. Wöls, I. B. H. Wilson, V. Sladek, M. Hajdúch, M. Poláková and J. Kóňa, *ChemMedChem*, 2018, **13**, 373–383.
17 T. Klunda, S. Šesták, J. Kóňa and M. Poláková, *Bioorg. Chem.*, 2019, **83**, 424–431.
18 P. Heikinheimo, R. Helland, H.-K. S. Leiros, I. Leiros, S. Karlsen, G. Evjen, R. Ravelli, G. Schoehn, R. Ruigrok, O.-K. Tollersrud, S. McSweeney and E. Hough, *J. Mol. Biol.*, 2003, **327**, 631–644.
19 E.-L. Tsou, Y.-T. Yeh, P.-H. Liang and W.-C. Cheng, *Tetrahedron*, 2009, **65**, 93–100.
20 W.-A. Chen, A. Sayyad, C.-W. Chen, Y.-H. Chen, T.-J. R. Cheng and W.-C. Cheng, *Asian J. Org. Chem.*, 2019, **8**, 2233–2242.
21 W.-C. Cheng, C.-W. Guo, C.-K. Lin and Y.-R. Jiang, *Isr. J. Chem.*, 2015, **55**, 403–411.
22 L. Li, Z. Chen, X. Zhang and Y. Jia, *Chem. Rev.*, 2018, **118**, 3752–3832.
23 J.-S. Zhu, S. Nakagawa, W. Chen, I. Adachi, Y.-M. Jia, X.-G. Hu, G. W. J. Fleet, F. X. Wilson, T. Nitoda, G. Horne, R. van Well, A. Kato and C.-Y. Yu, *J. Org. Chem.*, 2013, **78**, 10298–10309.
24 M. Bessodes, D. Komiotis and K. Antonakis, *Tetrahedron Lett.*, 1986, **27**, 579–580.
25 A. Mengel and O. Reiser, *Chem. Rev.*, 1999, **99**, 1191–1224.
26 S. C. Nigama, A. Mann, M. Taddei and C.-G. Wermutha, *Synth. Commun.*, 1989, **19**, 3139–3142.
27 W. Yu, Y. Mei, Y. Kang, Z. Hua and Z. Jin, *Org. Lett.*, 2004, **6**, 3217–3219.
28 R. Singh, M. K. Parai, S. Mondal and G. Panda, *Synth. Commun.*, 2013, **43**, 253–259.
29 C.-Y. Wu, C.-F. Chang, J. S.-Y. Chen, C.-H. Wong and C.-H. Lin, *Angew. Chem., Int. Ed.*, 2003, **42**, 4661–4664.
30 H. Fiaux, D. A. Kuntz, D. Hoffman, R. C. Janzer, S. Gerber-Lemaire, D. R. Rose and L. Juillerat-Jeanneret, *Bioorg. Med. Chem.*, 2008, **16**, 7337–7346.
31 T. Kuribara, M. Hirano, G. Speciale, S. J. Williams, Y. Ito and K. Totani, *ChemBioChem*, 2017, **18**, 1027–1035.
32 J. C. Bigge, T. P. Patel, J. A. Bruce, P. N. Goulding, S. M. Charles and R. B. Parekh, *Anal. Biochem.*, 1995, **230**, 229–238.
33 R. Chen, M. A. Pawlicki, B. S. Hamilton and T. J. Tolbert, *Adv. Synth. Catal.*, 2008, **350**, 1689–1695.
34 S. al Daher, R. de Gasperi, P. Daniel, N. Hall, C. D. Warren and B. Winchester, *Biochem. J.*, 1991, **277**, 743–751.
35 I. Cenci di Bello, P. Dorling and B. Winchester, *Biochem. J.*, 1983, **215**, 693–696.

36 I. Cenci di Bello, G. Fleet, S. K. Namgoong, K. I. Tadano and B. Winchester, *Biochem. J.*, 1989, **259**, 855–861.
37 J.-C. Michalski and A. Klein, *Biochim. Biophys. Acta, Mol. Basis Dis.*, 1999, **1455**, 69–84.
38 S. Abdul Rahman, E. Bergström, C. J. Watson, K. M. Wilson, D. A. Ashford, J. R. Thomas, D. Ungar and J. E. Thomas-Oates, *J. Proteome Res.*, 2014, **13**, 1167–1176.
39 R. D. Cummings, A. G. Darvill, M. E. Etzler, *et al.*, *Essentials of Glycobiology*, ed. A. Varki, R. D. Cummings, J. D. Esko, *et al.*, Cold Spring Harbor Laboratory Press, Cold Spring Harbor (NY), 3rd edn, 2015, ch. 48.
40 D. O. Croci, J. P. Cerliani, T. Dalotto-Moreno, S. P. Méndez-Huergo, I. D. Mascanfroni, S. Dergan-Dylon, M. A. Toscano, J. J. Caramelo, J. J. García-Vallejo, J. Ouyang, E. A. Mesri, M. R. Junttila, C. Bais, M. A. Shipp, M. Salatino and G. A. Rabinovich, *Cell*, 2014, **156**, 744–758.
41 S. K. Patnaik, B. Potvin, S. Carlsson, D. Sturm, H. Leffler and P. Stanley, *Glycobiology*, 2005, **16**, 305–317.
42 A. Huang, X.-R. Yang, W.-Y. Chung, A. R. Dennison and J. Zhou, *Signal Transduction Targeted Ther.*, 2020, **5**, 146.
43 C.-W. Li, S.-O. Lim, E. M. Chung, Y.-S. Kim, A. H. Park, J. Yao, J.-H. Cha, W. Xia, L.-C. Chan, T. Kim, S.-S. Chang, H.-H. Lee, C.-K. Chou, Y.-L. Liu, H.-C. Yeh, E. P. Perillo, A. K. Dunn, C.-W. Kuo, K.-H. Khoo, J. L. Hsu, Y. Wu, J.-M. Hsu, H. Yamaguchi, T.-H. Huang, A. A. Sahin, G. N. Hortobagyi, S. S. Yoo and M.-C. Hung, *Cancer Cell*, 2018, **33**, 187–201.
44 S. Shi, S. Gu, T. Han, W. Zhang, L. Huang, Z. Li, D. Pan, J. Fu, J. Ge, M. Brown, P. Zhang, P. Jiang, K. W. Wucherpfennig and X. S. Liu, *Clin. Cancer Res.*, 2020, **26**, 5990.
45 L. Sun, C.-W. Li, E. M. Chung, R. Yang, Y.-S. Kim, A. H. Park, Y.-J. Lai, Y. Yang, Y.-H. Wang, J. Liu, Y. Qiu, K.-H. Khoo, J. Yao, J. L. Hsu, J.-H. Cha, L.-C. Chan, J.-M. Hsu, H.-H. Lee, S. S. Yoo and M.-C. Hung, *Cancer Res.*, 2020, **80**, 2298.